submitted to *Geophys. J. Int.*

Sensitivity kernels for body tides on laterally heterogeneous planets based on adjoint methods

Harriet C.P. Lau[1] and David Al-Attar[2]
[1]*Department of Earth and Planetary Science, University of California, Berkeley, CA 94720, USA*
[2]*Bullard Laboratories, Department of Earth Sciences, University of Cambridge, Cambridge CB3 OEZ, UK.*

SUMMARY

We apply the adjoint method to efficiently calculate the linearized sensitivity of body tide observations to perturbations in density, elastic/anelastic moduli, and boundary topography. This theory is implemented practically within the context of normal mode coupling calculations, with an advantage of this approach being that much of the necessary technical machinery is present in existing coupling codes. A range of example sensitivity kernels are calculated relative to both spherically symmetric and laterally heterogeneous background models. These results reaffirm the conclusions of earlier studies that the M2 body tide is strongly sensitive to spherical harmonic degree-2 density variations at the base of the mantle. Moreover, it is found that the sensitivity kernels are only weakly dependent on the background model, and hence linearized methods are likely to be effective within inversions of body tide observations.

Key words: Structure of the Earth; Tides and planetary waves; Inverse Theory; Tomography; Theoretical seismology; Surface waves and free oscillations

1 INTRODUCTION

Global seismic tomography has provided much insight into Earth's interior over the last few decades (e.g., Woodhouse & Dziewonski 1984; Ritsema et al. 1999; Masters et al. 2000; French & Romanowicz 2015; Bozdağ et al. 2016). Collectively, these studies have revealed increasingly resolved images

of Earth's seismic velocity field. At the lowest frequencies (towards time scales on the order of minutes and hours), the seismic response becomes increasingly sensitive to not only these velocity variations but also Earth's density and anelastic structure (Karato 1993; Dahlen & Tromp 1998). Tomographic models derived from this part of the seismic spectrum, i.e., normal modes or free oscillations, have offered new constraints on lateral variations on the Earth's density field from the earliest of such studies in the late nineties (Ishii & Tromp 1999).

Earth's density field represents just one example of an ill-constrained quantity vital to understanding the past and ongoing dynamics of mantle circulation and thus accurate determination of it remains a major goal in global geophysics. More recently, efforts towards this end have undergone a revival. For example, Moulik & Ekström (2016), with an expanded free oscillation data set, and Koelemeijer et al. (2017), with a special subset of free oscillations, namely Stoneley modes, have shown the potential to shed new light on mantle density. Moving to even lower frequencies (towards time scales on the order of hours to years), this trend of increasing sensitivity to density continues to Earth's body tides, or solid Earth tides. Lau et al. (2017), through the analysis of global GPS measurements of the body tide, tested several models of mantle buoyancy – based on seismic tomography models – and found regions of the deep mantle to be anomalously denser than surrounding mantle. Similar studies have investigated the body tide response of a laterally heterogeneous planet (e.g., Dehant et al. 1999; Métivier et al. 2006; Métivier & Conrad 2008; Latychev et al. 2009; Qin et al. 2014). These efforts represent growing availability of long period data. In particular, GPS measurements of body tidal displacement which are accurate to sub-millimeters (e.g., Yuan & Chao 2012; Yuan et al. 2013; Martens et al. 2016), and, potentially, wideband seismic data which can also detect tidal acceleration (e.g., Davis & Berger 2007). Such availability paves the way to further studies into the density, and, possibly, the anelatic structure of Earth's interior.

While these studies have demonstrated much potential in estimating Earth's density field, several methodological shortcomings mean that the robustness of density constraints can still be improved. In particular, the free oscillation studies discussed above (Ishii & Tromp 1999; Moulik & Ekström 2016; Koelemeijer et al. 2017) used mode coupling approximations in their forward calculations that have been shown to introduce significant inaccuracies in modeled spectra (Deuss & Woodhouse 2001; Al-Attar et al. 2012; Yang & Tromp 2015), with the latter studies advocating instead the application of so-called full mode couling approaches. Indeed, for the body tide application, Lau et al. (2015) showed that full mode coupling was absolutely necessary in order to accurately capture the body tide response on a laterally heterogeneous Earth and, as such, Lau et al. (2017) could not make use of such approximations.

Though Lau et al. (2017) did not make such approximations in the coupling of their modes, none

of these recent studies have accurately calculated the sensitivity of these long period data to Earth models with laterally hetergeneous structure. The existence of lateral heterogeneity at scales that are important for these data are well-studied (see, e.g., Garnero & McNamara 2008, for a review). Indeed, the sensitivity of data to model parameters has a deep connection with inverse methods. In many inverse problems, the gradient of data misfit with respect to model parameters of interest is required in order to find the combination of model parameters that minimize the misfit. Such gradient-based optimization methods are widely used in global geophysics.

The determination of such kernels and/or gradients, however, can be computationally demanding: consider a laterally heterogeneous model parameterized by n_ℓ spherical harmonic degrees and n_d radial basis functions. The total number of these spatial parameters, n_λ, is $(n_\ell + 1)^2 n_d$. If one were to use a finite difference scheme to calculate the sensitivity of the long period data to the density of the mantle at these spatial wavelengths, $n_\lambda + 1$ forward calculations would be required. As an example, for the seismic tomographic model S20RTS (Ritsema et al. 1999) $n_\ell = 20$ and $n_d = 21$, and so in order to achieve this for such a model 9262 forward calculations are required. Within the tidal application, sensitivity kernels for surface loads were explored by, e.g., Martens et al. (2016), for ocean tidal loads for a spherically symmetric Earth and we note that the theory herein may be extended for a surface load (see Crawford et al. 2018).

In recent years, the growing need of calculating Fréchet kernels with respect to a large number of model parameters for several geophysical applications has been met by the adoption of the so-called 'adjoint method'. For example, Liu & Tromp (2006) and Fichtner et al. (2006) have derived the method for seismic wave propagation, while for post-seismic and post-glacial relaxation applications, the theory has been derived by Crawford et al. (2017) and Crawford et al. (2018), respectively. Indeed, several seismology groups have successfully applied the adjoint methodology for seismic tomography (e.g., Tromp et al. 2005; Liu & Tromp 2008; Tape et al. 2010; Fichtner et al. 2009; Zhu et al. 2012). The adjoint method has roots within the field of optimal control (e.g., Lions 1971; Tröltzsch 2010) whereby exact gradients may be calculated through the determination of the forward solution and the associated adjoint solution. The latter calculation, in most cases, being closely related to the former. The combination of these two solutions provides the gradient with respect to any number of model parameters. In the case of S20RTS described above, the 9262 calculations required is reduced to two calculations. Furthermore, the adjoint method provides an ideal framework by which to directly invert for seismic spectra in a full mode coupling context, relinquishing the need to determine splitting functions. Thus, the advantage of the adjoint method is clear and has been demonstrated in numerous applications (e.g., Tromp et al. 2005; Liu & Tromp 2008; Tape et al. 2010; Fichtner et al. 2009; Zhu et al. 2012).

In this theoretical study, we apply the adjoint method to the body tide problem and in a future study we extend this to free oscillation seismology. The theory for both processes are intimately connected (Gilbert 1971; Wahr 1981; Lau et al. 2015) and hence so too is the adjoint framework. In what follows begin first by summarizing the equations of motion. We then introduce the forward problem and derive the adjoint problem, and include discussions on examples of sensitivity kernels and the practicalities of computing them. This theory deals only with semi-diurnal and long period tides. Diurnal tides involve additional resonances associated with free-core nutation, as described by Wahr (1981). This does not represent a fundamental limitation of the theory, but a substantial development computationally and will be a subject of further work.

2 EQUATIONS OF MOTION

We begin by recalling the equations of motion for the linearized deformation of a laterally heterogeneous, self-gravitating, elastic planet relative to a steadily rotating reference frame (e.g., Woodhouse & Dahlen 1978; Wahr 1981). These equations are common to studies of both body tides and free oscillations, but their form will be specialized to time-harmonic tidal problems later in Section 3. Having done this, linear viscoelastic effects can be incorporated in a simple manner using Boltzmann's superposition principle. Adapting slightly the notation used within Chapter 7 of Dahlen & Tromp (1998), the weak form of the equations of motion can be written

$$\langle\, \mathbf{u}' \,|P|\, \ddot{\mathbf{u}} \,\rangle + \langle\, \mathbf{u}' \,|W|\, \dot{\mathbf{u}} \,\rangle + \langle\, \mathbf{u}' \,|H|\, \mathbf{u} \,\rangle = \langle\, \mathbf{u}' \,|\, \mathbf{f} \,\rangle, \tag{2.1}$$

where $\mathbf{u}$ is the displacement vector field, over-letter dots are used to denote time-differentiation, $\mathbf{u}'$ is a sufficiently regular time-independent test-function, $\mathbf{f}$ is an applied body force, and the three terms on the left hand side are, respectively, sesquilinear forms associated with inertial, Coriolis, and elasto-gravitational forces that are described further below. Here we are using a variant of Dirac's bra-ket notation such that the right hand side denotes the inner product

$$\langle\, \mathbf{u}' \,|\, \mathbf{f} \,\rangle = \int_M \overline{\mathbf{u}'(\mathbf{x})} \cdot \mathbf{f}(\mathbf{x}, t)\, \mathrm{d}^3\mathbf{x}, \tag{2.2}$$

where $M \subseteq \mathbb{R}^3$ is the volume occupied by the planet at equilibrium, complex conjugation is indicated by an overline, and we write $\cdot$ to denote the pointwise Euclidean inner product of two vectors. The inertial form is given by

$$\langle\, \mathbf{u}' \,|P|\, \mathbf{u} \,\rangle = \int_M \rho\, \overline{\mathbf{u}'} \cdot \mathbf{u}\, \mathrm{d}^3\mathbf{x}, \tag{2.3}$$

where ρ is the planet's equilibrium density field. This sesquilinear form is readily seen to be Hermitian, meaning that

$$\langle\, \mathbf{u}' \,|P|\, \mathbf{u} \,\rangle = \overline{\langle\, \mathbf{u} \,|P|\, \mathbf{u}' \,\rangle} \tag{2.4}$$

for all $\mathbf{u}'$ and $\mathbf{u}$, and is also positive-definite so that $\langle\, \mathbf{u}\,|P|\,\mathbf{u}\,\rangle > 0$ for all non-zero $\mathbf{u}$. The Coriolis form is defined as

$$\langle\, \mathbf{u}'\,|W|\,\mathbf{u}\,\rangle = \int_M 2\rho\,\overline{\mathbf{u}'}\cdot(\boldsymbol{\Omega}\times\mathbf{u})\,\mathrm{d}^3\mathbf{x}, \tag{2.5}$$

where $\boldsymbol{\Omega}$ is the equilibrium value of the planet's angular velocity. This form is anti-Hermitian, meaning that

$$\langle\, \mathbf{u}'\,|W|\,\mathbf{u}\,\rangle = -\overline{\langle\, \mathbf{u}\,|W|\,\mathbf{u}'\,\rangle}, \tag{2.6}$$

for all $\mathbf{u}'$ and $\mathbf{u}$. Finally, the elasto-gravitational form is given by

$$\begin{aligned}\langle\, \mathbf{u}'\,|H|\,\mathbf{u}\,\rangle = &\int_M \nabla\overline{\mathbf{u}'} : \boldsymbol{\Lambda} : \nabla\mathbf{u}\,\mathrm{d}^3\mathbf{x} + \frac{1}{2}\int_M \rho\,(\overline{\mathbf{u}'}\cdot\nabla\phi + \mathbf{u}\cdot\nabla\overline{\phi'})\,\mathrm{d}^3\mathbf{x}\\ &+\int_M \rho\,\overline{\mathbf{u}'}\cdot\nabla\nabla(\Phi+\psi)\cdot\mathbf{u}\,\mathrm{d}^3\mathbf{x}\\ &+\frac{1}{2}\int_{\Sigma_{\mathrm{FS}}} \varpi\left[\overline{\mathbf{u}'}\cdot(\nabla_\Sigma\mathbf{u})\cdot\mathbf{n} + \mathbf{u}\cdot(\nabla_\Sigma\overline{\mathbf{u}'})\cdot\mathbf{n}\right]\mathrm{d}\Sigma\\ &-\frac{1}{2}\int_{\Sigma_{\mathrm{FS}}} \left[(\mathbf{n}\cdot\overline{\mathbf{u}'})\nabla_\Sigma\cdot(\varpi\mathbf{u}) + (\mathbf{n}\cdot\mathbf{u})\nabla_\Sigma\cdot(\varpi\overline{\mathbf{u}'})\right]\mathrm{d}\Sigma,\end{aligned} \tag{2.7}$$

where $\boldsymbol{\Lambda}$ is the elastic tensor relating the linearizations of the deformation gradient and first Piola-Kirchhoff stress tensor; ϕ is the Eulerian perturbation to the gravitational potential associated with the displcement vector $\mathbf{u}$, and ϕ' is the corresponding quantity determined from the test function $\mathbf{u}'$; Φ is the equilibrium value of the planet's gravitational potential; ψ is the centrifugal potential associated with the steadily rotating reference frame; ϖ is the equilibrium pressure on fluid solid boundaries, with the union of these surfaces being denoted by Σ_{FS}, their outward unit normals written $\mathbf{n}$, and ∇_Σ being the associated tangential gradient operator. Aspherical structure implies the existence of deviatoric pre-stress. It is not clear what the appropriate values for such pre-stress would be and Dahlen (1972) showed that such stresses could be neglected over the much larger isotropic stresses. However, the theory is sufficiently general to incorporate non-hydrostatic pre-stress both within the elastic tensor and the continuity conditions on fluid-solid boundaries Woodhouse & Dahlen (1978).

An explicit expression (e.g., Dahlen & Tromp 1998, Chapter 3) for the gravitational potential perturbation's gradient $\nabla\phi$ in terms of the displacement vector field $\mathbf{u}$ is given by

$$(\nabla\phi)(\mathbf{x},t) = G\int_M \rho(\mathbf{x}')\,\boldsymbol{\Pi}(\mathbf{x}-\mathbf{x}')\cdot\mathbf{u}(\mathbf{x}',t)\,\mathrm{d}^3\mathbf{x}', \tag{2.8}$$

where G is the gravitational constant, and the integral kernel is

$$\boldsymbol{\Pi}(\mathbf{x}) = \frac{\mathbf{1}}{\|\mathbf{x}\|^3} - \frac{3\mathbf{x}\otimes\mathbf{x}}{\|\mathbf{x}\|^5}, \tag{2.9}$$

while an identical formula relates for the test function $\mathbf{u}'$ to $\nabla\phi'$. Using the pointwise symmetry $\Lambda_{ijkl} = \Lambda_{klij}$, which follows from the existence of a strain-energy function, along with eq. (2.7) and (2.8), it can be seen that the elasto-gravitational form is Hermitian. As a final comment, within the

weak formulation of the problem both the displacement vector field and test function must be continuous across solid-solid boundaries, while on fluid-solid boundaries Σ_{FS} we impose the tangential slip constraints

$$[\mathbf{n}\cdot\mathbf{u}]^{+}_{-}=0, \quad \left[\mathbf{n}\cdot\mathbf{u}'\right]^{+}_{-}=0. \tag{2.10}$$

Dynamical boundary and continuity conditions on the linearized traction vector are, however, incorporated automatically within the weak formulation, and so need not be imposed explicitly on the displacement vector field.

3 BODY TIDE THEORY

3.1 Reduction to a time-harmonic problem

For body tides the appropriate force term in eq. (2.1) is given by

$$\mathbf{f}=\rho\nabla\psi \tag{3.1}$$

where $\psi(\mathbf{x},t)$ is a time-dependent tidal potential. If the planet has an ocean, this potential will also generate ocean tides that couple to the internal deformation. We will not account for ocean tides within this work, and instead assume that, when present, their effects have been subtracted from observations to a sufficient level of accuracy (e.g., Lau et al. 2017). A general tidal potential can be usefully decomposed into a sum of time-harmonic terms (e.g., Agnew 2015), and by linearity of the equations of motion we may focus on a single tidal species with angular frequency $\omega\in\mathbb{R}$. Given this assumption, the applied body force takes the simpler form

$$\mathbf{f}=\mathrm{Re}[\,\rho\nabla\tilde{\psi}\mathrm{e}^{\mathrm{i}\omega t}\,], \tag{3.2}$$

where $\tilde{\psi}(\mathbf{x})$ is a complex-valued tidal potential amplitude. The corresponding steady-state displacement vector is then given by

$$\mathbf{u}=\mathrm{Re}[\,\tilde{\mathbf{u}}\,\mathrm{e}^{\mathrm{i}\omega t}\,], \tag{3.3}$$

where $\tilde{\mathbf{u}}(\mathbf{x})$ is a complex-valued displacement amplitude. Substituting these time-harmonic expresions for the body force and displacement field into eq. (2.1) and cancelling the common exponential factors, we arrive at the steady-state problem

$$-\omega^2\langle\,\mathbf{u}'\,|P|\,\tilde{\mathbf{u}}\,\rangle+\mathrm{i}\omega\langle\,\mathbf{u}'\,|W|\,\tilde{\mathbf{u}}\,\rangle+\langle\,\mathbf{u}'\,|H|\,\tilde{\mathbf{u}}\,\rangle=\langle\,\mathbf{u}'\,|\,\rho\nabla\tilde{\psi}\,\rangle. \tag{3.4}$$

At this stage, linear viscoelastic effects can be incorporated in a simple manner through the use of Boltzmann's superposition principle (e.g., Dahlen & Tromp 1998, Chapter 6). Indeed, we need only replace the elastic tensor $\mathbf{\Lambda}(\mathbf{x})$ occuring within the elasto-gravitational form with an appropriate

complex-valued and frequency-dependent viscoelastic tensor that will be denoted $\tilde{\mathbf{\Lambda}}(\mathbf{x},\omega)$. To indicate this modification, we re-write the steady-state equations of motion in eq. (3.4) as

$$-\omega^2\langle\,\mathbf{u}'\,|P|\,\tilde{\mathbf{u}}\,\rangle+\mathrm{i}\omega\langle\,\mathbf{u}'\,|W|\,\tilde{\mathbf{u}}\,\rangle+\langle\,\mathbf{u}'\,|H(\omega)|\,\tilde{\mathbf{u}}\,\rangle=\langle\,\mathbf{u}'\,|\,\rho\nabla\tilde{\psi}\,\rangle, \tag{3.5}$$

where the final sesquilinear form has an explicit frequency-dependence through the dependence of H on the viscoelastic tensor $\tilde{\mathbf{\Lambda}}$. It can be shown (e.g., Dahlen & Tromp 1998, Chapter 6) that $\omega\mapsto\tilde{\mathbf{\Lambda}}(\mathbf{x},\omega)$ is a holomorphic function within the lower half of the complex plane (i.e. $\mathrm{Im}\,\omega<0$), and that

$$\overline{\tilde{\mathbf{\Lambda}}(\mathbf{x},\omega)}=\tilde{\mathbf{\Lambda}}(\mathbf{x},-\overline{\omega}), \tag{3.6}$$

for all $\omega\in\mathbb{C}$ for which $\tilde{\mathbf{\Lambda}}$ is well-defined (where in the textbook of Dahlen & Tromp (1998), this frequency is denoted ν). Note that in the viscoelastic case we retain the pointwise symmetry $\tilde{\Lambda}_{ijkl}=\tilde{\Lambda}_{klij}$, the physical basis for this assumption being discussed by Day (1971a,b). Using these properties, it follows easily that the Hermitian symmetry of the elasto-gravitational form generalizes to the identity

$$\langle\,\mathbf{u}'\,|H(\omega)|\,\mathbf{u}\,\rangle=\overline{\langle\,\mathbf{u}\,|H(-\overline{\omega})|\,\mathbf{u}'\,\rangle}, \tag{3.7}$$

which holds for all $\mathbf{u}'$ and $\mathbf{u}$, and any $\omega\in\mathbb{C}$ for which the viscoelastic tensor is well-defined at each $\mathbf{x}\in M$. At this stage, it is convenient to define the frequency-dependent sesquilinear form

$$\langle\,\mathbf{u}'\,|S(\omega)|\,\tilde{\mathbf{u}}\,\rangle=-\omega^2\langle\,\mathbf{u}'\,|P|\,\tilde{\mathbf{u}}\,\rangle+\mathrm{i}\omega\langle\,\mathbf{u}'\,|W|\,\tilde{\mathbf{u}}\,\rangle+\langle\,\mathbf{u}'\,|H(\omega)|\,\tilde{\mathbf{u}}\,\rangle, \tag{3.8}$$

which, from the above discussion, satisfies

$$\langle\,\mathbf{u}'\,|S(\omega)|\,\mathbf{u}\,\rangle=\overline{\langle\,\mathbf{u}\,|S(-\overline{\omega})|\,\mathbf{u}'\,\rangle}, \tag{3.9}$$

for any $\mathbf{u}'$ and $\mathbf{u}$, and all suitable $\omega\in\mathbb{C}$. With this notation, eq. (3.5) can be written more concisely as

$$\langle\,\mathbf{u}'\,|S(\omega)|\,\tilde{\mathbf{u}}\,\rangle=\langle\,\mathbf{u}'\,|\,\rho\nabla\tilde{\psi}\,\rangle, \tag{3.10}$$

with the equality, as ever, being required to hold for all suitable test functions $\mathbf{u}'$. The tidal problem in eq. (3.10) admits a unique solution so long as the forcing frequency $\omega\in\mathbb{R}$ is not equal to one of the planet's eigenfrequencies. We need not discuss this issue in any detail for the moment, and it will simply be assumed within this section that the condition is met. Indeed, tidal frequencies are generally much smaller than those of seismic free oscillations, and so this is a fairly safe assumption. The one caveat is that if the planet has a fluid core, then a tidal frequency might be at or close to resonance with rotational modes such as the nearly diurnal free wobble (Smith 1977) or with core undertones (Rogister & Valette 2009). While our theory is, in principle, sufficiently general to account for near resonance phenomena, numerical calculations become significantly more challenging. As a result, we

later consider only semi-diurnal and long-period tides, and neglect the excitation of core undertones within normal mode coupling calculations.

3.2 Sensitivity kernels for body tides

3.2.1 Objective functionals and sensitivity kernels

Consider a real-valued function J defined in terms of the displacement amplitude field $\tilde{\mathbf{u}}$ for a single tidal species with frequency $\omega \in \mathbb{R}$. For example, suppose we have estimated point-values $\tilde{\mathbf{u}}_i$ of the displacement amplitude for this tide at a set of surface locations $\mathbf{x}_i \in \partial M$, $i = 1, \dots, N$. Given a model for the planet's structure, we can calculate predicted values $\tilde{\mathbf{u}}(\mathbf{x}_i)$ for these displacement amplitudes by solving eq. (3.10), and then quantify their fit with the observations as

$$J = \sum_{i=1}^{N} \frac{1}{2N\sigma_i^2} \|\tilde{\mathbf{u}}(\mathbf{x}_i) - \tilde{\mathbf{u}}_i\|^2, \tag{3.11}$$

where the σ_i are appropriate standard errors, and $\|\cdot\|$ denotes the usual norm in $\mathbb{C}^3$.

The displacement amplitude $\tilde{\mathbf{u}}$ depends on the planetary structure in a complicated manner through the solution of eq. (3.10), and so the objective functional J implicitly depends on this structure. Our aim is to obtain sensitivity kernels relating first-order perturbations in the planetary structure to the resulting first-order perturbation in such objective functionals. For example, if we perturb the planet's equilibrium density to $\rho + \delta\rho$ while holding all other parameters constant, then we expect a first-order accurate relation of the form

$$\delta J = \int_M K_\rho \, \delta\rho \, \mathrm{d}^3\mathbf{x}, \tag{3.12}$$

with K_ρ being, by definition, the sensitivity kernel for density. Corresponding sensitivity kernels can be introduced for tensor-valued model parameters like the elastic tensor, or those, such as boundary topography, defined on surfaces within the planet.

3.2.2 The adjoint body tide problem

As before, we let J denote a real-valued objective functional defined in terms of $\tilde{\mathbf{u}}$. If the displacement amplitude is perturbed to $\tilde{\mathbf{u}} + \delta\tilde{\mathbf{u}}$, we assume that the resulting first-order change in J can be written in the form

$$\delta J = \mathrm{Re}\langle \tilde{\mathbf{h}} \,|\, \delta\tilde{\mathbf{u}} \rangle, \tag{3.13}$$

where $\tilde{\mathbf{h}}$ is a vector-valued function. For example, perturbing the objective functional defined in eq. (3.11), we find

$$\delta J = \mathrm{Re} \sum_{i=1}^{N} \frac{1}{N\sigma_i^2} \overline{[\tilde{\mathbf{u}}(\mathbf{x}_i) - \tilde{\mathbf{u}}_i]} \cdot \delta\mathbf{u}(\mathbf{x}_i), \tag{3.14}$$

and this can be placed into the required form by setting

$$\tilde{\mathbf{h}}(\mathbf{x}) = \frac{1}{N} \sum_{i=1}^{N} \frac{1}{\sigma_i^2} [\tilde{\mathbf{u}}(\mathbf{x}_i) - \tilde{\mathbf{u}}_i] \delta(\mathbf{x} - \mathbf{x}_i), \tag{3.15}$$

with $\delta(\mathbf{x})$ the Dirac delta function. We now perturb to first-order accuracy the equations of motion in eq. (3.10) to obtain

$$\langle\, \mathbf{u}' \,|S(\omega)|\, \delta\tilde{\mathbf{u}} \,\rangle + \langle\, \mathbf{u}' \,|\delta S(\omega)|\, \tilde{\mathbf{u}} \,\rangle = \langle\, \mathbf{u}' \,|\, \delta\rho\nabla\tilde{\psi} \,\rangle, \tag{3.16}$$

where the sesquilinear form $\langle\, \mathbf{u}' \,|\delta S(\omega)|\, \tilde{\mathbf{u}} \,\rangle$ is defined in the obvious manner in terms of the given model perturbations. Motivated by eq. (3.13), suppose that the following identity

$$\langle\, \mathbf{u}' \,|S(\omega)|\, \delta\tilde{\mathbf{u}} \,\rangle = \langle\, \tilde{\mathbf{h}} \,|\, \delta\tilde{\mathbf{u}} \,\rangle, \tag{3.17}$$

were to hold for all possible values of $\delta\tilde{\mathbf{u}}$. This condition defines an equation for $\mathbf{u}'$ in weak form that we discuss further below. We can now combine eqs (3.16) and (3.17) and use eq.(3.13) to arrive at the key result

$$\delta J = \mathrm{Re}[\langle\, \mathbf{u}' \,|\, \delta\rho\nabla\tilde{\psi} \,\rangle - \langle\, \mathbf{u}' \,|\delta S(\omega)|\, \tilde{\mathbf{u}} \,\rangle], \tag{3.18}$$

in which the first-order perturbation to the displacement amplitude field has been eliminated. Eq. (3.17) is the adjoint body tide problem, with $\mathbf{u}'$ playing the role of the adjoint variable.

To clarify this approach it will be useful to modify our notations slightly. First, from eq. (3.9) we note that eq. (3.17) can be equivalently written in a form closer to eq. (3.10) as

$$\langle\, \delta\tilde{\mathbf{u}} \,|S(-\omega)|\, \mathbf{u}' \,\rangle = \langle\, \delta\tilde{\mathbf{u}} \,|\, \tilde{\mathbf{h}} \,\rangle, \tag{3.19}$$

where we have used the fact that tidal frequencies are real-valued, and again emphasise that in this context $\delta\tilde{\mathbf{u}}$ acts as an arbitrary test-function. Finally, for notational symmetry, we define

$$\tilde{\mathbf{h}}^\dagger = -\tilde{\mathbf{h}}, \quad \tilde{\mathbf{u}}^\dagger = -\mathbf{u}', \tag{3.20}$$

so that eq. (3.19) becomes

$$\langle\, \delta\tilde{\mathbf{u}} \,|S(-\omega)|\, \tilde{\mathbf{u}}^\dagger \,\rangle = \langle\, \delta\tilde{\mathbf{u}} \,|\, \tilde{\mathbf{h}}^\dagger \,\rangle, \tag{3.21}$$

while our expression for δJ can be written

$$\delta J = \mathrm{Re}[\langle\, \tilde{\mathbf{u}}^\dagger \,|\delta S(\omega)|\, \tilde{\mathbf{u}} \,\rangle - \langle\, \tilde{\mathbf{u}}^\dagger \,|\, \delta\rho\nabla\tilde{\psi} \,\rangle]. \tag{3.22}$$

We can now summarize the process by which the sensitivity kernels are calculated. First, we solve eq. (3.10) to determine the displacement amplitude field $\tilde{\mathbf{u}}$. Using this field, we calculate J along with the corresponding *adjoint force* $\tilde{\mathbf{h}}^\dagger$. We can then solve the *adjoint body tide problem* defined in

eq. (3.21) to obtain the *adjoint displacement amplitude field* $\tilde{\mathbf{u}}^\dagger$. Here we note that the adjoint body tide problem closely resembles the forward problem in eq. (3.10); in fact, in an elastic and non-rotating planet they coincide exactly. Once we have both the forward and adjoint displacement amplitides $\tilde{\mathbf{u}}$ and $\tilde{\mathbf{u}}^\dagger$, we can substitute them into eq. (3.22) and simply extract the sensitivity kernels for each model parameter. To illustrate this latter point, consider an elastic planet in which we have perturbed the elastic tensor to $\boldsymbol{\Lambda} + \delta\boldsymbol{\Lambda}$ while holding all other model parameters constant. It is then clear from eq. (2.7) and (3.22) that

$$\delta J = \mathrm{Re} \int_M \overline{\nabla \tilde{\mathbf{u}}^\dagger} : \delta\boldsymbol{\Lambda} : \nabla \tilde{\mathbf{u}} \, \mathrm{d}^3\mathbf{x}, \tag{3.23}$$

and hence using eq. (3.22) we can identify the appropriate sensitivity kernel as a fourth-order tensor field

$$\mathbf{K}_{\boldsymbol{\Lambda}} = \mathrm{Re}\Big[\overline{\nabla \tilde{\mathbf{u}}^\dagger} \otimes \nabla \tilde{\mathbf{u}} \Big] , \tag{3.24}$$

where $\otimes$ denotes the tensor product. Using index notation this expression can be equivalently written as

$$[\mathbf{K}_{\boldsymbol{\Lambda}}]_{ijkl} = \mathrm{Re}\Big[\overline{\partial_i \tilde{u}_j^\dagger} \, \partial_k \tilde{u}_l \Big] . \tag{3.25}$$

Using the adjoint method, corresponding sensitivity kernels can be similarly obtained for other model parameters such as density, boundary topography, or those associated with viscoelastic rheologies. Appropriate expressions for these terms, as derived in Woodhouse & Dahlen (1978), may be found summarized in Dahlen & Tromp (1998). We postpone statement of such results until the next subsection.

3.3 Implementation in the context of mode coupling calculations

As shown by Lau et al. (2015), normal mode coupling theory provides an accurate and efficient method for calculating body tides within laterally heterogeneous planetary models. In this section, we show how the adjoint method described can be practically implemented within this context. A major advantage of this approach is that almost all of the necessary theoretical expressions have been derived and are readily implemented into coupling codes (see Dahlen & Tromp 1998). In the following discussion, however, we introduce some further assumptions and approximations to simplify the presentation. First, we restrict attention to isotropic and elastic planets. Next, we follow standard practice in free oscillation seismology by neglecting any deviatoric component of the equilibrium stress, while accounting for the effects of lateral density variations and aspherical boundary topography only up to first-order accuracy within the sequilinear form $\langle \, \mathbf{u}' \, | S(\omega) | \, \mathbf{u} \, \rangle$. The extension of our methods to anisotropic and/or viscoelastic planets is straightforward, but more work is required to account fully

for lateral density variations and/or boundary topography within coupling calculations – see Al-Attar et al. (2018) for a possible route forward.

Given these assumptions, the three volumetric model parameters we consider are then the shear μ and bulk κ modulii along with the density ρ. To describe aspherical boundary topography, suppose that the radii of internal and external boundaries in the reference planet are denoted by a_i with i ranging over a finite indexing set. Each reference boundary is then perturbed such that its radius is given by

$$r = a_i + h_i, \tag{3.26}$$

with the boundary topography h_i a function on the unit two-sphere. Considering perturbations $(\delta\mu, \delta\kappa, \delta\rho, \delta h_1, \delta h_2, \ldots)$ to these model parameters, we can expand their angular dependence in spherical harmonics as

$$\delta\mu = \sum_{st} \delta\mu_{st}\, Y^0_{st}, \quad \delta\kappa = \sum_{st} \delta\kappa_{st}\, Y^0_{st}, \quad \delta\rho = \sum_{st} \delta\rho_{st}\, Y^0_{st}, \quad \delta h_i = \sum_{st} \delta h_{i,st}\, Y^0_{st}, \tag{3.27}$$

where Y^N_{st} denotes a generalized spherical harmonic of degree s, order t, and upper index N, these functions being normalized according to the conventions within Appendix C of (Dahlen & Tromp 1998). Note that as the shear modulus perturbation $\delta\mu$ is real-valued its expansion coefficients must possess the symmetry $\overline{\delta\mu_{st}} = (-1)^t \delta\mu_{s-t}$, with analogous results holding for the other model parameters.

The basic idea underlying mode coupling calculations is the expansion of the displacement amplitude $\tilde{\mathbf{u}}$ using the eigenfunctions of a spherically symmetric, non-rotating, and elastic reference planet. Such an expansion is possible because these eigenfunctions form a complete orthonormal basis for vector fields in the planetary model (here we ignore complications associated with the existence of a fluid core). Within numerical work it is, of course, necessary to truncate the expansion to some finite-basis set, but by including sufficiently many terms, the calculations can be made as accurate as desired (e.g., Akbarashrafi et al. 2017). Within the reference planetary model, the eigenvalue problem that defines its eigenfunctions $\mathbf{u}$ and eigenfrequencies ω can be written

$$-\omega^2 \langle\, \mathbf{u}' \,|P_0|\, \mathbf{u} \,\rangle + \langle\, \mathbf{u}' \,|H_0|\, \mathbf{u} \,\rangle = 0, \tag{3.28}$$

where $\mathbf{u}'$ is again a test-function, and we have added subscript 0 to the sesquilinear forms associated with the reference planet. The Hermitian symmetry of the two sesquilinear forms occurring in this problem implies that the squared eigenfrequencies are real-valued, and we will assume that the planet is gravitationally stable, so that all squared-eigenfrencies are positive except for those at zero-frequency associated with rigid body translations and rotations. Due to the planet's spherical symmetry, each eigenfunction can be labeled with four integers (ℓ, m, n, p) with ℓ the angular degree, m the angular order, n the overtone number, and p an index used to distinguish different mode types (e.g.,

spheroidal, toroidal, inner core toroidal). The corresponding eigenfrequency $\omega_{\ell np}$ is independent of m, and so each eigenfunction belongs to a $(2\ell+1)$-fold degenerate multiplet. Following Woodhouse (1980), we will simplify notations by combining (ℓ, n, p) into a single index k. We can then denote the appropriate eigenfrequency by ω_k, and the eigenfunctions by $|\, km \,\rangle$ where again we use bra-ket notation. Eigenfunctions lying in distinct multiplets are necessarily pair-wise orthogonal relative to the inertial form, meaning that

$$\langle\, km \,|P_0|\, k'm' \,\rangle = 0, \tag{3.29}$$

while we are free to choose a basis for each degenerate multiplet such that the orthonormalization condition

$$\langle\, km \,|P_0|\, k'm' \,\rangle = \delta_{kk'}\delta_{mm'}, \tag{3.30}$$

holds.

Given this preamble, we can expand the displacement amplitude as

$$\tilde{\mathbf{u}} = \sum_{k'm'} \langle\, k'm' \,|P_0|\, \tilde{\mathbf{u}} \,\rangle |\, k'm' \,\rangle, \tag{3.31}$$

and substituting into eq. (3.10) we find

$$\sum_{k'm'} \langle\, km \,|S(\omega)|\, k'm' \,\rangle \langle\, k'm' \,|P_0|\, \tilde{\mathbf{u}} \,\rangle = \langle\, km \,|\, \rho\nabla\tilde{\psi} \,\rangle, \tag{3.32}$$

where we have taken the test function to equal $|\, km \,\rangle$. Due to the completeness of the reference eigenfunctions, eq. (3.32) holding for all indices (k, m) is equivalent to the weak formulation of the body tide problem discussed previously. This equation can be understood as an infinite-dimensional set of linear algebraic equations that determine the expansion coefficients $\langle\, k'm' \,|P_0|\, \tilde{\mathbf{u}} \,\rangle$ of the displacement amplitude field. A corresponding expansion can be made for the adjoint displacement amplitude field $\tilde{\mathbf{u}}^\dagger$, and from eq. (3.21) we readily obtain

$$\sum_{k'm'} \langle\, km \,|S(-\omega)|\, k'm' \,\rangle \langle\, k'm' \,|P_0|\, \tilde{\mathbf{u}}^\dagger \,\rangle = \langle\, km \,|\, \tilde{\mathbf{h}}^\dagger \,\rangle, \tag{3.33}$$

for the adjoint body tide problem. By suitably truncating both eqs (3.32) and (3.33) we arrive at finite-dimensional systems of linear equations that can be either solved using direct methods based on techniques like LU-decomposition when the size of the system is not too large (e.g., Hara et al. 1993), or otherwise through iterative matrix-free approaches (e.g., Al-Attar et al. 2012).

Turning to the calculation of sensitivity kernels, we simply substitute the above expansions for the forward and adjoint displacement amplitude fields into eq. (3.22) to obtain

$$\delta J = \mathrm{Re} \sum_{km} \sum_{k'm'} \langle\, \tilde{\mathbf{u}}^\dagger \,|P_0|\, km \,\rangle \langle\, km \,|\delta S(\omega)|\, k'm' \,\rangle \langle\, k'm' \,|P_0|\, \tilde{\mathbf{u}} \,\rangle$$

$$-\mathrm{Re}\sum_{km}\langle\,\tilde{\mathbf{u}}^{\dagger}\,|P_0|\,km\,\rangle\langle\,km\,|\,\delta\rho\nabla\tilde{\psi}\,\rangle. \tag{3.34}$$

Only the density perturbation contributes to the final term on the right hand side, and this will be dealt with separately below. For the moment we focus attention on the perturbed matrix elements $\langle\,km\,|\delta S(\omega)|\,k'm'\,\rangle$ occurring within eq. (3.34). As discussed within Woodhouse (1980), the Wigner-Eckart theorem implies that the perturbed matrix elements takes the form

$$\langle\,km\,|\delta S(\omega)|\,k'm'\,\rangle = \sum_{st}(-1)^{m+l}\begin{pmatrix}\ell & s & \ell'\\ -m & t & m'\end{pmatrix}\langle\,k\,||\delta S(\omega)||\,k'\,\rangle_{st}, \tag{3.35}$$

where the array denotes a Wigner-3j symbol (e.g., Edmonds 1960). The terms $\langle\,k\,||\delta S(\omega)||\,k'\,\rangle_{st}$ within this expression, which are independent of the orders m and m', are known as reduced matrix elements and Woodhouse (1980) showed that they can be written

$$\begin{aligned}\langle\,k\,||\delta S(\omega)||\,k'\,\rangle_{st} = (-1)^{l}4\pi\nu_\ell\nu_s\nu_{\ell'}\,\times\\ \left[\int_0^a\left(K_\mu^{ksk'}\,\delta\mu_{st}+K_\kappa^{ksk'}\,\delta\kappa_{st}+K_\rho^{ksk'}\,\delta\rho_{st}\right)r^2\,\mathrm{d}r\right.\\ \left.+\sum_i K_i^{ksk'}\delta h_{i,st}\,a_i^2\right],\end{aligned} \tag{3.36}$$

where $\nu_\ell=\sqrt{\frac{2\ell+1}{4\pi}}$, a is the planet's radius, and the radial functions $K_\mu^{ksk'}$, $K_\kappa^{ksk'}$, $K_\rho^{ksk'}$, and the coefficients $K_i^{ksk'}$ are now known as Woodhouse kernels, with their form being tabulated in the literature (e.g., Woodhouse 1980; Mochizuki 1986; Dahlen & Tromp 1998).

To simplify the discussion, it will be useful to temporalily set all model perturbations except for that of the shear modulus equal to zero. We can then combine the above results to write

$$\begin{aligned}\delta J = \mathrm{Re}\sum_{km}\sum_{k'm'}\sum_{st}(-1)^m 4\pi\nu_\ell\nu_s\nu_{\ell'}\begin{pmatrix}\ell & s & \ell'\\ -m & t & m'\end{pmatrix}\times\\ \langle\,\tilde{\mathbf{u}}^{\dagger}\,|P_0|\,km\,\rangle\langle\,k'm'\,|P_0|\,\tilde{\mathbf{u}}\,\rangle\int_0^a K_\mu^{ksk'}\,\delta\mu_{st}r^2\,\mathrm{d}r.\end{aligned} \tag{3.37}$$

Collecting terms appropriately, this becomes

$$\delta J = \mathrm{Re}\sum_{st}\int_0^a \overline{K_\mu^{st}}\,\delta\mu_{st}r^2\,\mathrm{d}r, \tag{3.38}$$

where for each spherical harmonic degree and order we have defined the radial kernels

$$K_\mu^{st} = \sum_{km}\sum_{k'm'}(-1)^m 4\pi\nu_\ell\nu_s\nu_{\ell'}\begin{pmatrix}\ell & s & \ell'\\ -m & t & m'\end{pmatrix}\langle\,km\,|P_0|\,\tilde{\mathbf{u}}^{\dagger}\,\rangle\langle\,\tilde{\mathbf{u}}\,|P_0|\,k'm'\,\rangle\overline{K_\mu^{ksk'}}. \tag{3.39}$$

Within eq. (3.38) we can insert the spherical harmonic orthogonality condition

$$\delta_{ss'}\delta_{tt'} = \int_{\mathbb{S}^2}\overline{Y_{s't'}^0}Y_{st}^0\,\mathrm{d}S, \tag{3.40}$$

to obtain

$$\delta J \;=\; \mathrm{Re}\sum_{s't'}\sum_{st}\int_{\mathbb{S}^2}\overline{Y_{s't'}^0}Y_{st}^0\,\mathrm{d}S\int_0^a\overline{K_\mu^{s't'}}\,\delta\mu_{st}r^2\,\mathrm{d}r$$

$$
\begin{aligned}
&= \mathrm{Re}\int_0^a \int_{\mathbb{S}^2} \overline{\sum_{s't'} K_\mu^{s't'} Y_{s't'}^0} \sum_{st} \delta\mu_{st} Y_{st}^0 r^2 \,\mathrm{d}S\,\mathrm{d}r \\
&= \int_M \left(\mathrm{Re}\sum_{s't'} K_\mu^{s't'} Y_{s't'}^0 \right) \delta\mu \,\mathrm{d}^3\mathbf{x}, \qquad (3.41)
\end{aligned}
$$

where in establishing the second equality we have used the fact that $\delta\mu$ is real-valued. It follows that the sensitivity kernel for μ can be written in the form of a spherical harmonic expansion

$$
K_\mu = \sum_{st} \frac{1}{2} \left[K_\mu^{st} + (-1)^t \overline{K_\mu^{s-t}} \right] Y_{st}^0 \qquad (3.42)
$$

where from eq. (3.39) we see that the radial expansion coefficients are formed from appropriate weightings of the Woodhouse kernels for shear modulus using the coefficients obtained within both the forward and adjoint body tide problems. Exactly the same ideas apply to the kernels for bulk modulus and boundary topography, and we obtain

$$
K_\kappa = \sum_{st} \frac{1}{2} \left[K_\kappa^{st} + (-1)^t \overline{K_\kappa^{s-t}} \right] Y_{st}^0, \qquad (3.43)
$$

$$
K_i = \sum_{st} \frac{1}{2} \left[K_i^{st} + (-1)^t \overline{K_i^{s-t}} \right] Y_{st}^0, \qquad (3.44)
$$

with the coefficients K_κ^{st} and K_i^{st} defined as in eq. (3.39) but with the Woodhouse kernels for μ replaced by those for the appropriate model parameter. In the case of density we need to account for the second term in eq. (3.34), and by inspection arrive at

$$
K_\rho = \sum_{st} \frac{1}{2} \left[K_\rho^{st} + (-1)^t \overline{K_\rho^{s-t}} \right] Y_{st}^0 - \mathrm{Re}\sum_{km} \langle\, \tilde{\mathbf{u}}^\dagger \,|P_0|\, km \,\rangle \overline{|\, km \,\rangle} \cdot \nabla\tilde{\psi}, \qquad (3.45)
$$

with the coefficients K_ρ^{st} again being defined by analogy with eq. (3.39). The spatially varying parts $\overline{|\, km \,\rangle} \cdot \nabla\tilde{\psi}$ of the final term in this expression can also be conveniently reduced to the form of a spherical harmonic expansion (see eq. (70) of Lau et al. 2015).

3.4 Application

3.4.1 Truncation of the adjoint problem within practical calculations

Before proceeding to calculate sensitivity kernels, we explore sensible means of truncating the expansions in expressions (3.32) and (3.33). These truncations are dictated by two factors: the forcing geometry and how highly resolved we would like our sensitivity kernels to be (of course, the two are related).

An advantage of the tidal problem is that the dominant forcings lie in a few distinct spatial geometries, the largest of which occurs at $\ell = 2$ (note that the semi-diurnal constituent, $m = 2$, is by far the largest "degree-2" tide and so we will turn our attention to this single tidal harmonic). This vastly reduces the expansions required. Fig. 1 shows how structural perturbations of $\{s, t\}$ harmonic

Spheroidal modes, ${}_n\mathcal{S}_\ell$, included for perturbations up to degree 6 ($s \leq 6$):
${}_0\mathcal{S}_2, {}_2\mathcal{S}_1, {}_0\mathcal{S}_3, {}_0\mathcal{S}_4, {}_1\mathcal{S}_2, {}_0\mathcal{S}_0, {}_0\mathcal{S}_5, {}_1\mathcal{S}_3, {}_2\mathcal{S}_2, {}_3\mathcal{S}_1, {}_0\mathcal{S}_6, {}_3\mathcal{S}_2, {}_1\mathcal{S}_4, {}_0\mathcal{S}_7, {}_2\mathcal{S}_3,$ ${}_1\mathcal{S}_5, {}_2\mathcal{S}_4, {}_4\mathcal{S}_1, {}_0\mathcal{S}_8, {}_3\mathcal{S}_3, {}_2\mathcal{S}_5, {}_1\mathcal{S}_6, {}_1\mathcal{S}_0, {}_1\mathcal{S}_7, {}_2\mathcal{S}_6, {}_5\mathcal{S}_1, {}_4\mathcal{S}_2, {}_1\mathcal{S}_8, {}_3\mathcal{S}_4, {}_2\mathcal{S}_7,$ ${}_6\mathcal{S}_1, {}_2\mathcal{S}_8, {}_4\mathcal{S}_3, {}_5\mathcal{S}_2, {}_5\mathcal{S}_3, {}_7\mathcal{S}_1, {}_3\mathcal{S}_5, {}_4\mathcal{S}_4, {}_5\mathcal{S}_4, {}_4\mathcal{S}_5, {}_6\mathcal{S}_2, {}_2\mathcal{S}_0, {}_7\mathcal{S}_2, {}_3\mathcal{S}_6, {}_4\mathcal{S}_6,$ ${}_3\mathcal{S}_7, {}_5\mathcal{S}_5, {}_3\mathcal{S}_8, {}_6\mathcal{S}_3, {}_8\mathcal{S}_1$

Table 1. Spheroidal modes included in all tidal calculations listed in increasing eigenfrequency.

contribute to the kernel with depth, folding all orders t into a single s-dependent quantity, α_M^s, where $\alpha_M^s = \sum_{t=-s}^{t=+s} K_M^{st}/(2s+1)$. As can be seen, beyond structural perturbations of degree two ($s = 2$), sensitivity for all model parameters decreases drastically. As such, in the following examples we do not consider spatial perturbations greater than $s = 6$. In the examples below we will mainly focus on spherically symmetric earth models (though will include a laterally heterogeneous example). For such an earth model, we can use the following selection rule to dictate how far the adjoint modes will couple

$$|\ell_\psi - s| \leq \ell_\dagger \leq \ell_\psi + s, \tag{3.46}$$

where ℓ_ψ and s are the spherical harmonic degrees of the forward problem forcing and the volumetric perturbation considered, and $\ell_\dagger$ is the adjoint degree for which coupling will occur. If we were interested in considering the sensitivity of the body tide to volumetric perturbations of $s \leq 20$, we would then expand expressions (3.32) and (3.33) to $\ell = 22$. When calculating kernels relative to a laterally heterogeneous background model this approach ceases to be exact as a tidal force at degree ℓ_ψ will produce a response containing higher degrees. Nonetheless, because lateral variations are in practice expected to be small, the above truncation scheme provides a useful starting point.

We also note that the presence of the delta-function in eq. (3.15) may be expanded as follows

$$\delta(\mathbf{x} - \mathbf{x}') = \delta(r - r') \sum_{\ell=0}^{\ell=\infty} \sum_{m=-\ell}^{m=\ell} \overline{Y}_{\ell m}(\theta', \phi') Y_{\ell m}(\theta, \phi), \tag{3.47}$$

where θ, ϕ, and r are the colatitude, longitude and radius, respectively. Truncation will produce the Gibbs effect and in order to reduce this, we apply the modified expression

$$\delta(\mathbf{x} - \mathbf{x}') \approx \delta(r - r') \sum_{\ell=0}^{\ell=L} \sum_{m=-\ell}^{m=\ell} \exp\left(-2\pi \frac{\ell+1}{L+\frac{1}{2}}\right) \overline{Y}_{\ell m}(\theta', \phi') Y_{\ell m}(\theta, \phi), \tag{3.48}$$

where L is the maximum degree of truncation (see Appendix E of Al-Attar & Tromp 2014).

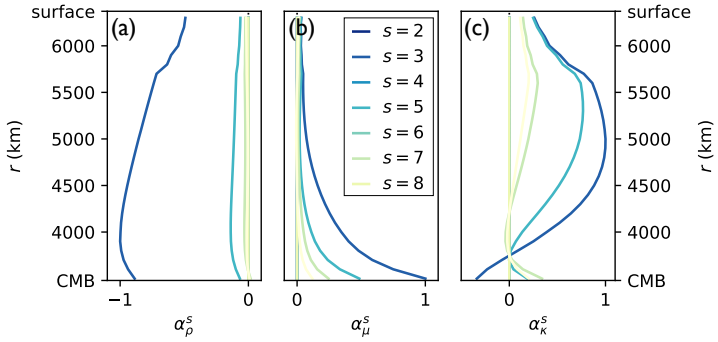

Figure 1. Depth dependent kernels for perturbations of degree s in density (a), shear (b), and bulk moduli (c), assuming a background model PREM (Dziewonski & Anderson 1981) and coupling modes listed in Table 1, where $\alpha^s_M = \sum_{t=-s}^{t=+s} K^{st}_M/(2s+1)$. All kernels within each panel are normalized.

3.4.2 Numerical Examples of Sensitivity Kernels

Following Section 3.3 we summarize the expression for any given kernel associated with the model perturbation δM as

$$K_M = \mathrm{Re} \sum_{st} \left[\sum_{km} \sum_{k'm'} (-1)^m 4\pi \nu_l \nu_s \nu_{l'} \begin{pmatrix} l & s & l' \\ -m & t & m' \end{pmatrix} \times \right.$$
$$\left. \langle\, km \,|P_0|\, \tilde{\mathbf{u}}^\dagger \,\rangle \langle\, \tilde{\mathbf{u}} \,|P_0|\, k'm' \,\rangle \overline{K^{ksk'}_M} \right] Y^0_{st}. \tag{3.49}$$

The first stage is to determine both $\tilde{\mathbf{u}}$ by forcing the equation of motion with the tidal force and $\tilde{\mathbf{u}}^\dagger$ by forcing the suitably modified equation of motion with a point source located at the position of our observation. Our chosen observation is the vertical displacement. In these examples, we used eigenfunctions and eigenfrequencies of a spherically symmetric, non-rotating, elastic, and isotropic (i.e., "SNREI") Earth (in which case $W \to 0$ and H includes no dissipative or dispersive effects) as our SNREI basis, calculated using the software package MINEOS (Masters et al. 2011). The basis modes included in our coupling calculations are listed in Table 1 and we adopt the density and elastic structure of the "Preliminary Reference Earth Model" (Dziewonski & Anderson 1981). While we include only spheroidal modes, toroidal modes are easily incorporated, though for our chosen observation, the coupling of toroidal modes is negligible and the truncation of higher frequency modes leads to satisfactory results. The calculations we present are intended for demonstrative purposes. We note that all the sensitivity calculations to follow are associated with the ampltide of the vertical displacement of the body tide.

The first set of calculations concern the depth dependent sensitivity kernels and were previously introduced to justify our truncation (Fig. 1), though we expand here. Following the truncation in eq. (3.46) and including modes whose reference eigenfrequencies are less than 3 mHz, we fully couple

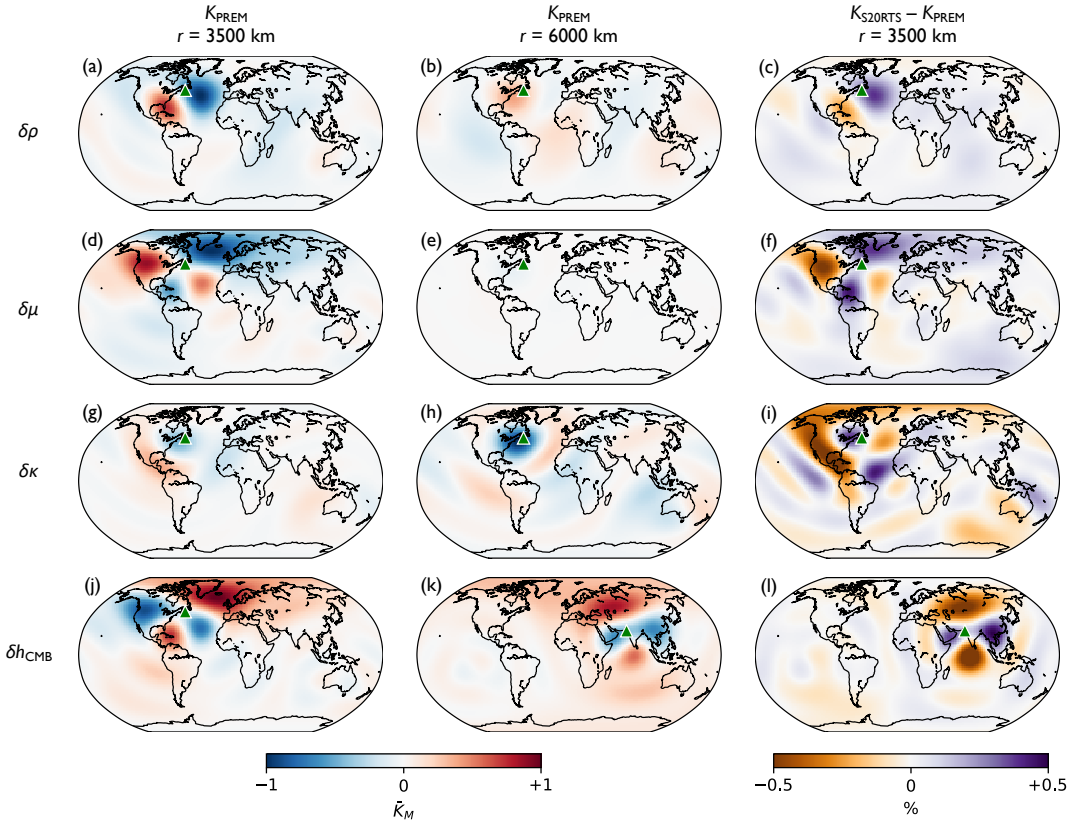

Figure 2. Sensitivity kernels of the vertical displacement of the body tide located at the green triangle to perturbations in density, ρ (panels a-c), the shear modulus, μ (panels d-f), the bulk modulus, κ (panels g-i), topography along the CMB, $_{\rm CMB}$ (panels j-i). For ρ, μ, and κ, the first (panels a,d,g) and second (panels b,e,h) columns are kernels at a radii of 3500 km and 6000 km, respectively, computed using the 1D background model PREM (Dziewonski & Anderson 1981). The third column (panels c,f,i) displays the percent difference in these kernels at $r = 3500$ km when calculated with the 3D model S40RTS (Ritsema et al. 2011). For $h_{\rm CMB}$, panels j and k are the kernels, computed assuming PREM, for two different measurement locations and panel l is the percent difference between the kernel shown in panel k and the same but calculated assuming S40RTS. All kernels are normalized for each model parameter.

the modes listed in Table 1. While we have presented kernels for each order t individually, the resulting depth profiles in Fig. 1 provide interesting information concerning the depth sensitivity of each model parameter. (These kernels have been normalized for each parameter, across all $\{s, t\}$ kernels.) As can be seen, both density and shear modulus have much of their sensitivity in the deep mantle. This is in accord with results in Lau et al. (2015) where a finite-difference approach was used to investigate sensitivity.

In addition, Fig. 2 shows the spatial variability of K_M for observations at a single point on Earth's surface (marked by green triangles) for volumetric model perturbations in ρ, μ, and κ (top three rows), and two locations for the boundary topograhy at the CMB, $h_{\rm CMB}$ (bottom row). The volumetric pertur-

bations are displayed at two radii (3500 km and 6000 km) (left two columns). These were determined for spatial perturbations up to and including degree 6 (i.e., $0 \leq s \leq 6$). As such, with the truncation rule in eq. (3.46) and including modes whose reference eigenfrequencies are less than 3 mHz, the modes that were coupled are listed in Table 1. Panels (a,b), (d,e), (g,h), and (j,k) show perturbations the spherically symmetric background model PREM, K_{PREM}. The kernels are normalized across each model perturbation.

Fig. 2 demonstrates how the forward and adjoint fields interact where the deep mantle sensitivity is laterally smeared but focuses to a more localized region towards the surface, centered at the measurement location. In other words, sensitivity broadens to longer wavelengths moving closer to the core-mantle boundary, as the geometry of the body tide force dominates the pattern of sensitivity. As with the depth profiles (Fig. 1), perturbations in ρ and μ are largest towards the base of the mantle, while for κ, the opposite is true.

Finally, we computed 3D sensitivity kernels in the same manner. The background v_{s} model used was S40RTS (Ritsema et al. 2011) and we applied uniform scaling values of 0.4 and 0.1 to map perturbations in v_{s} to perturbations in v_ρ and v_{b}, respectively. We have presented the differences between these 3D and 1D calculations in the right column of Fig. 2 in percentages for only the kernel field at $r = 3500$ km (panels c,f,i). For the CMB topography differences, we show only the kernel associated with the location at panel (k). As can be seen, the differences between the kernals are less than one percent. This reflects the linear nature of this problem and that 1D kernels may be sufficient if we expect small perturbations in model parameters. This may not be the case if large perturbations in model parameters exist, e.g., the small zones in the deep mantle of ultra-low velocity (the so-called ULVZs that exhibit shear wave-speed anomalies as low as $\sim$30%; McNamara et al. 2010), though their small size likely means their effect on tides will be negligible (Fig. 1).

4 CONCLUSIONS

In this study we present a methodology to calculate sensitivity kernels for the body tide problem via the adjoint method. These kernels may be calculated with equal ease relative to a background 1D or 3D model. In the examples we show, we use mode coupling as the basis of determining the kernels, building upon expressions that have already been derived within free oscillation theory (e.g., Woodhouse 1980; Dahlen & Tromp 1998). From our examples, it can be seen that the background models of PREM (spherically symmetric; Dziewonski & Anderson 1981) and S40RTS (spherically asymmetric; Ritsema et al. 2011) result in very similar kernels. While this may be the case for models in which perturbations are not too far from the spherically symmetric case, incorporating much larger anomalies may result in significant deviation between 3D and 1D kernels.

DATA AVAILABILITY

The software used for all calculations within in this article will be shared on reasonable request to the corresponding author.

ACKNOWLEDGMENTS

HL would like to acknowledge support from NSF grant EAR-1923865. HL and DA equally contributed to the results presented in this manuscript.

REFERENCES

Agnew, D., 2015. Earth tides, in *Treatise on Geophysics (Second Edition)*, pp. 151 – 178, ed. Schubert, G., Elsevier, Oxford, second edition edn.

Akbarashrafi, F., Al-Attar, D., Deuss, A., Trampert, J., & Valentine, A., 2017. Exact free oscillation spectra, splitting functions and the resolvability of earth's density structure, *Geophysical Journal International*, p. ggx539.

Al-Attar, D. & Tromp, J., 2014. Sensitivity kernels for viscoelastic loading based on adjoint methods, *Geophysical Journal International*, **196**, 34–77.

Al-Attar, D., Woodhouse, J. H., & Deuss, A., 2012. Calculation of normal mode spectra in laterally heterogeneous earth models using an iterative direct solution method, *Geophysical Journal International*, **189**(2), 1038–1046.

Al-Attar, D., Woodhouse, J. H., & Deuss, A., 2012. Calculation of normal mode spectra in laterally heterogeneous earth models using an iterative direct solution method, *Geophysical Journal International*, **189**(2), 1038–1046.

Al-Attar, D., Crawford, O., Valentine, A. P., & Trampert, J., 2018. Hamilton's principle and normal mode coupling in an aspherical planet with a fluid core, *Geophysical Journal International*, **214**(1), 485–507.

Bozdağ, E., Peter, D., Lefebvre, M., Komatitsch, D., Tromp, J., Hill, J., Podhorszki, N., & Pugmire, D., 2016. Global adjoint tomography: first-generation model, *Geophysical Journal International*, **207**(3), 1739–1766.

Crawford, O., Al-Attar, D., Tromp, J., & Mitrovica, J. X., 2017. Forward and inverse modelling of post-seismic deformation, *Geophysical Journal International*, **208**, 845–876.

Crawford, O., Al-Attar, D., Tromp, J., Mitrovica, J. X., Austermann, J., & Lau, H. C., 2018. Quantifying the sensitivity of post-glacial sea level change to laterally varying viscosity, *Geophysical journal international*, **214**(2), 1324–1363.

Dahlen, F. A., 1972. Elastic velocity anisotropy in the presence of an anisotropic initial stress, *Bulletin of the Seismological Society of America*, **62**(5), 1183–1193.

Dahlen, F. A. & Tromp, J., 1998. *Theoretical Global Seismology*, Princeton University Press.

Davis, J. P. & Berger, J., 2007. Calibration of the Global Seismographic Network Using Tides, *Seismological Research Letters*, **78**(4), 454–459.

Day, W. A., 1971a. Time-reversal and the symmetry of the relaxation function of a linear viscoelastic material, *Archive for Rational Mechanics and Analysis*, **40**(3), 155–159.

Day, W. A., 1971b. RESTRICTIONS ON RELAXATION FUNCTIONS IN LINEAR VISCOELASTICITY, *The Quarterly Journal of Mechanics and Applied Mathematics*, **24**(4), 487–497.

Dehant, V., Defraigne, P., & Wahr, J. M., 1999. Tides for a Convective Earth, *Journal of Geophysical Research*, **104**(B1), 1035.

Deuss, A. & Woodhouse, J. H., 2001. Theoretical free-oscillation spectra: the importance of wide band coupling, *Geophysical Journal International*, **146**, 833–842.

Dziewonski, A. M. & Anderson, D. L., 1981. Preliminary reference Earth model, *Physics of the Earth and Planetary Interiors*, **25**(4), 297–356.

Edmonds, A. R., 1960. *Angular Momentum in Quantum Mechanics*, Princeton University Press.

Fichtner, A., Bunge, H.-P., & Igel, H., 2006. The adjoint method in seismology. I. Theory, *Physics of the Earth and Planetary Interiors*, **157**, 86–104.

Fichtner, A., Kennett, B. L. N., Igel, H., & Bunge, H.-P., 2009. Full seismic waveform tomography for upper-mantle structure in the Australasian region using adjoint methods, *Geophysical Journal International*, **179**, 1703–1725.

French, S. W. & Romanowicz, B., 2015. Broad plumes rooted at the base of the Earth's mantle beneath major hotspots, *Nature*, **525**(7567), 95–99.

Garnero, E. J. & McNamara, A. K., 2008. Structure and Dynamics of Earth's Lower Mantle, *Science*, **320**, 626.

Gilbert, F., 1971. Excitation of the Normal Modes of the Earth by Earthquake Sources, *Geophysical Journal International*, **22**(2), 223–226.

Hara, T., Tsuboi, S., & Geller, R. J., 1993. Inversion for laterally heterogeneous upper mantle S-wave velocity structure using iterative waveform inversion, *Geophysical Journal International*, **115**(3), 667–698.

Ishii, M. & Tromp, J., 1999. Normal-mode and free-air gravity constraints on lateral variations in velocity and density of earth's mantle, *Science*, **285**(5431), 1231–1236.

Karato, S.-I., 1993. Importance of anelasticity in the interpretation of seismic tomography, *Geophysical Research Letters*, **20**, 1623–1626.

Koelemeijer, P., Deuss, A., & Ritsema, J., 2017. Density structure of Earth's lowermost mantle from Stoneley mode splitting observations, *Nature Communications*, **8**, 15241.

Latychev, K., Mitrovica, J. X., Ishii, M., Chan, N.-H., & Davis, J. L., 2009. Body Tides on a 3-D Elastic Earth: Toward a Tidal Tomography, *Earth and Planetary Science Letters*, **277**(1-2), 86–90.

Lau, H. C., Yang, H.-Y., Tromp, J., Mitrovica, J. X., Latychev, K., & Al-Attar, D., 2015. A normal mode treatment of semi-diurnal body tides on an aspherical, rotating and anelastic Earth, *Geophysical Journal International*, **202**(2), 1392–1406.

Lau, H. C. P., Faul, U., Mitrovica, J. X., Al-Attar, D., Tromp, J., & Garapić, G., 2017. Anelasticity across seismic to tidal timescales: a self-consistent approach, *Geophysical Journal International*, **208**, 368–384.

Lions, J., 1971. *Optimal Control of Systems Governed by Partial Differential Equations*, Grundlehren der mathematischen Wissenschaften in Einzeldarstellungen mit besonderer Berücksichtigung der Anwendungsgebiete, Springer-Verlag.

Liu, Q. & Tromp, J., 2006. Finite-Frequency Kernels Based on Adjoint Methods, *The Bulletin of the Seismological Society of America*, **96**, 2383–2397.

Liu, Q. & Tromp, J., 2008. Finite-frequency sensitivity kernels for global seismic wave propagation based upon adjoint methods, *Geophysical Journal International*, **174**, 265–286.

Martens, H. R., Rivera, L., Simons, M., & Ito, T., 2016. The sensitivity of surface mass loading displacement response to perturbations in the elastic structure of the crust and mantle, *Journal of Geophysical Research (Solid Earth)*, **121**(5), 3911–3938.

Martens, H. R., Simons, M., Owen, S., & Rivera, L., 2016. Observations of ocean tidal load response in South America from subdaily GPS positions, *Geophysical Journal International*, **205**(3), 1637–1664.

Masters, G., Laske, G., Bolton, H., & Dziewonski, A., 2000. The relative behavior of shear velocity, bulk sound speed, and compressional velocity in the mantle: Implications for chemical and thermal structure, *Washington DC American Geophysical Union Geophysical Monograph Series*, **117**, 63–87.

Masters, G., Woodhouse, J. H., & Freeman, G., 2011. Mineos v1.0.2, computational infrastructure for geodynamics.

McNamara, A. K., Garnero, E. J., & Rost, S., 2010. Tracking deep mantle reservoirs with ultra-low velocity zones, *Earth and Planetary Science Letters*, **299**(1-2), 1–9.

Métivier, L. & Conrad, C. P., 2008. Body Tides of a Convecting, Laterally Heterogeneous, and Aspherical Earth, *Journal of Geophysical Research*, **113**(B11), B11405.

Mochizuki, E., 1986. The free oscillations of an anisotropic and heterogeneous earth., *Geophysical Journal*, **86**, 167–176.

Moulik, P. & Ekström, G., 2016. The relationships between large-scale variations in shear velocity, density, and compressional velocity in the Earth's mantle, *Journal of Geophysical Research (Solid Earth)*, **121**, 2737–2771.

Métivier, L., Greff-Lefftz, M., & Diament, M., 2006. Mantle lateral variations and elastogravitational deformations — I. Numerical modelling, *Geophysical Journal International*, **167**(3), 1060–1076.

Qin, C., Zhong, S., & Wahr, J., 2014. A Perturbation Method and its Application: Elastic Tidal Response of a Laterally Heterogeneous Planet, *Geophysical Journal International*, **199**(2), 631–647.

Ritsema, J., Heijst, H. J. v., & Woodhouse, J. H., 1999. Complex shear wave velocity structure imaged beneath africa and iceland, *Science*, **286**(5446), 1925–1928.

Ritsema, J., Deuss, A., van Heijst, H. J., & Woodhouse, J. H., 2011. S40RTS: a degree-40 shear-velocity model for the mantle from new Rayleigh wave dispersion, teleseismic traveltime and normal-mode splitting function measurements, *Geophysical Journal International*, **184**(3), 1223–1236.

Rogister, Y. & Valette, B., 2009. Influence of liquid core dynamics on rotational modes, *Geophysical Journal International*, **176**(2), 368–388.

Smith, M. L., 1977. Wobble and nutation of the earth, *Geophysical Journal*, **50**, 103–140.

Tape, C., Liu, Q., Maggi, A., & Tromp, J., 2010. Seismic tomography of the southern California crust based on spectral-element and adjoint methods, *Geophysical Journal International*, **180**, 433–462.

Tröltzsch, F., 2010. *Optimal Control of Partial Differential Equations: Theory, Methods, and Applications*, Graduate studies in mathematics, American Mathematical Society.

Tromp, J., Tape, C., & Liu, Q., 2005. Seismic tomography, adjoint methods, time reversal and banana-doughnut kernels, *Geophysical Journal International*, **160**, 195–216.

Wahr, J. M., 1981. Body tides on an elliptical, rotating, elastic and oceanless earth., *Geophysical Journal*, **64**, 677–703.

Wahr, J. M., 1981. A normal mode expansion for the forced response of a rotating earth, *Geophysical Journal of the Royal Astronomical Society*, **64**(3), 651–675.

Woodhouse, J. H., 1980. The Coupling and Attenuation of Nearly Resonant Multiplets in the Earth's Free Oscillation Spectrum, *Geophysical Journal International*, **61**(2), 261–283.

Woodhouse, J. H. & Dahlen, F. A., 1978. The Effect of a General Aspherical Perturbation on the Free Oscillations of the Earth, *Geophysical Journal International*, **53**(2), 335–354.

Woodhouse, J. H. & Dziewonski, A. M., 1984. Mapping the Upper Mantle: Three Dimensional Modeling of Earth Structure by Inversion of Seismic Waveforms, *Journal of Geophysical Research (Solid Earth)*, **89**, 5953–5986.

Yang, H.-Y. & Tromp, J., 2015. Synthetic free-oscillation spectra: an appraisal of various mode-coupling methods, *Geophysical Journal International*, **203**(2), 1179–1192.

Yuan, L. & Chao, B. F., 2012. Analysis of Tidal Signals in Surface Displacement Measured by a Dense Continuous GPS Array, *Earth and Planetary Science Letters*, **355-356**, 255–261.

Yuan, L., Chao, B. F., Ding, X., & Zhong, P., 2013. The tidal displacement field at Earth's surface determined using global GPS observations, *Journal of Geophysical Research (Solid Earth)*, **118**, 2618–2632.

Zhu, H., Bozdağ, E., Peter, D., & Tromp, J., 2012. Structure of the European upper mantle revealed by adjoint tomography, *Nature Geoscience*, **5**, 493–498.